Report

Neuron

Structural Insights into Modulation of Neurexin-Neuroligin *Trans*-synaptic Adhesion by MDGA1/ Neuroligin-2 Complex

Highlights

- Crystal structure of neuroligin-2 (NL2) in complex with MDGA1 Ig1-Ig3 domains
- MDGA1 Ig1-Ig2 domains interact with NL2 dimer with 2:2 stoichiometry
- MDGA1 competes with Nrx1β for NL2 binding via their overlapping binding site on NL2
- MDGA1 selectively forms complexes with NL2, but not NL1, in vivo

Authors

Jung A Kim, Doyoun Kim, Seoung Youn Won, ..., Jie-Oh Lee, Jaewon Ko, Ho Min Kim

Correspondence

jaewonko@dgist.ac.kr (J.K.), hm_kim@kaist.ac.kr (H.M.K.)

In Brief

Kim et al. investigated the crystal structure of 2:2 heterotetrameric neuroligin-2/MDGA1 complexes and the molecular mechanism underlying MDGA1-mediated inhibition of neuroligin-2 synaptogenic activity. MDGA1 specifically associates with neuroligin-2 in vivo, suggesting a mechanism that restricts interaction of MDGA1 with neuroligin-2.

Data Resources

5XEQ

Kim et al., 2017, Neuron *94*, 1121–1131
June 21, 2017
http://dx.doi.org/10.1016/j.neuron.2017.05.034

CellPress

Neuron
Report

Structural Insights into Modulation of Neurexin-Neuroligin *Trans*-synaptic Adhesion by MDGA1/Neuroligin-2 Complex

Jung A Kim,[1,8] Doyoun Kim,[2,8] Seoung Youn Won,[3] Kyung Ah Han,[4] Dongseok Park,[4] Eunju Cho,[4] Nayoung Yun,[5] Hyun Joo An,[5] Ji Won Um,[4] Eunjoon Kim,[2,6] Jie-Oh Lee,[3,9] Jaewon Ko,[4,9,*] and Ho Min Kim[2,7,9,10,*]
[1]Graduate School of Nanoscience and Technology, Korea Advanced Institute of Science and Technology (KAIST), Daejeon 34141, Korea
[2]Center for Synaptic Brain Dysfunctions, Institute for Basic Science, Daejeon 34141, Korea
[3]Department of Chemistry, KAIST, Daejeon 34141, Korea
[4]Department of Brain & Cognitive Sciences, Daegu Gyeongbuk Institute of Science and Technology (DGIST), Daegu 42988, Korea
[5]Graduate School of Analytical Science and Technology, Chungnam National University, Daejeon 305-764, Korea
[6]Department of Biological Sciences, KAIST, Daejeon 34141, Korea
[7]Graduate School of Medical Science & Engineering, KAIST, Daejeon 34141, Korea
[8]These authors contributed equally
[9]Senior author
[10]Lead Contact
*Correspondence: jaewonko@dgist.ac.kr (J.K.), hm_kim@kaist.ac.kr (H.M.K.)
http://dx.doi.org/10.1016/j.neuron.2017.05.034

SUMMARY

Membrane-associated mucin domain-containing glycosylphosphatidylinositol anchor proteins (MDGAs) bind directly to neuroligin-1 (NL1) and neuroligin-2 (NL2), thereby respectively regulating excitatory and inhibitory synapse development. However, the mechanisms by which MDGAs modulate NL activity to specify development of the two synapse types remain unclear. Here, we determined the crystal structures of human NL2/MDGA1 Ig1-3 complex, revealing their stable 2:2 arrangement with three interaction interfaces. Cell-based assays using structure-guided, site-directed MDGA1 mutants showed that all three contact patches were required for the MDGA's negative regulation of NL2-mediated synaptogenic activity. Furthermore, MDGA1 competed with neurexins for NL2 via its Ig1 domain. The binding affinities of both MDGA1 and MDGA2 for NL1 and NL2 were similar, consistent with the structural prediction of similar binding interfaces. However, MDGA1 selectively associated with NL2, but not NL1, in vivo. These findings collectively provide structural insights into the mechanism by which MDGAs negatively modulate synapse development governed by NLs/neurexins.

INTRODUCTION

Investigations into synaptogenesis mechanisms, orchestrated by a multitude of synaptic adhesion molecules, have yielded critical insights into synapse formation and function, as well as neural circuit shaping (Missler et al., 2012). Because many synaptic adhesion molecules are associated with human neurological and neuropsychiatric disorders, understanding the mechanistic actions of synaptic adhesion molecules in regulating distinct properties of various synapse and circuit types is clinically relevant (de la Torre-Ubieta et al., 2016). Studies have identified several potentially important synaptic adhesion molecules (i.e., synapse organizers) and have elucidated their functions in synapse formation, transmission, and plasticity (Um and Ko, 2013).

Neuroligins (NLs) are arguably the most widely studied class of postsynaptic adhesion molecules (Südhof, 2008). Genetic analyses using knockout mice deficient in individual NLs or combinations of NLs have shown that NLs dictate the properties of various synapse types across various brain regions (Bemben et al., 2015). Although all NL isoforms bind to presynaptic neurexins (Nrxs), albeit with different binding affinities, and to PDZ domain-containing proteins through their C-terminal ends, the synaptic localizations and functions of individual NLs are distinct (Krueger et al., 2012). In their native form, NLs exist as constitutive dimers, which induce the *trans*-synaptic clustering of Nrxs to positively regulate synaptic puncta size (Ko et al., 2009). Intriguingly, NL2 (an inhibitory synapse-specific NL isoform) exhibits unique biochemical properties, interacting specifically with gephyrin to regulate perisomatic inhibition, possibly through multiple intracellular phosphorylation events (Bemben et al., 2015). X-ray crystallography studies have significantly increased understanding of the binding between NLs and Nrxs, the modulation of these interactions by alternative splicing, and the involvement of Ca^{2+} ions in these interactions (Araç et al., 2007; Comoletti et al., 2010; Fabrichny et al., 2007; Leone et al., 2010).

The membrane-associated mucin (MAM) domain-containing GPI anchor protein 1 (MDGA1) was recently found to negatively regulate NL2-mediated synaptogenic activity through *cis*-configuration interaction (Lee et al., 2013; Pettem et al., 2013). Although NL2 also binds to MDGA2 in vitro, the role of MDGA2 at neuronal synapses remains unclear (Connor et al., 2016; Loh et al., 2016). One study using a proteomics-based approach

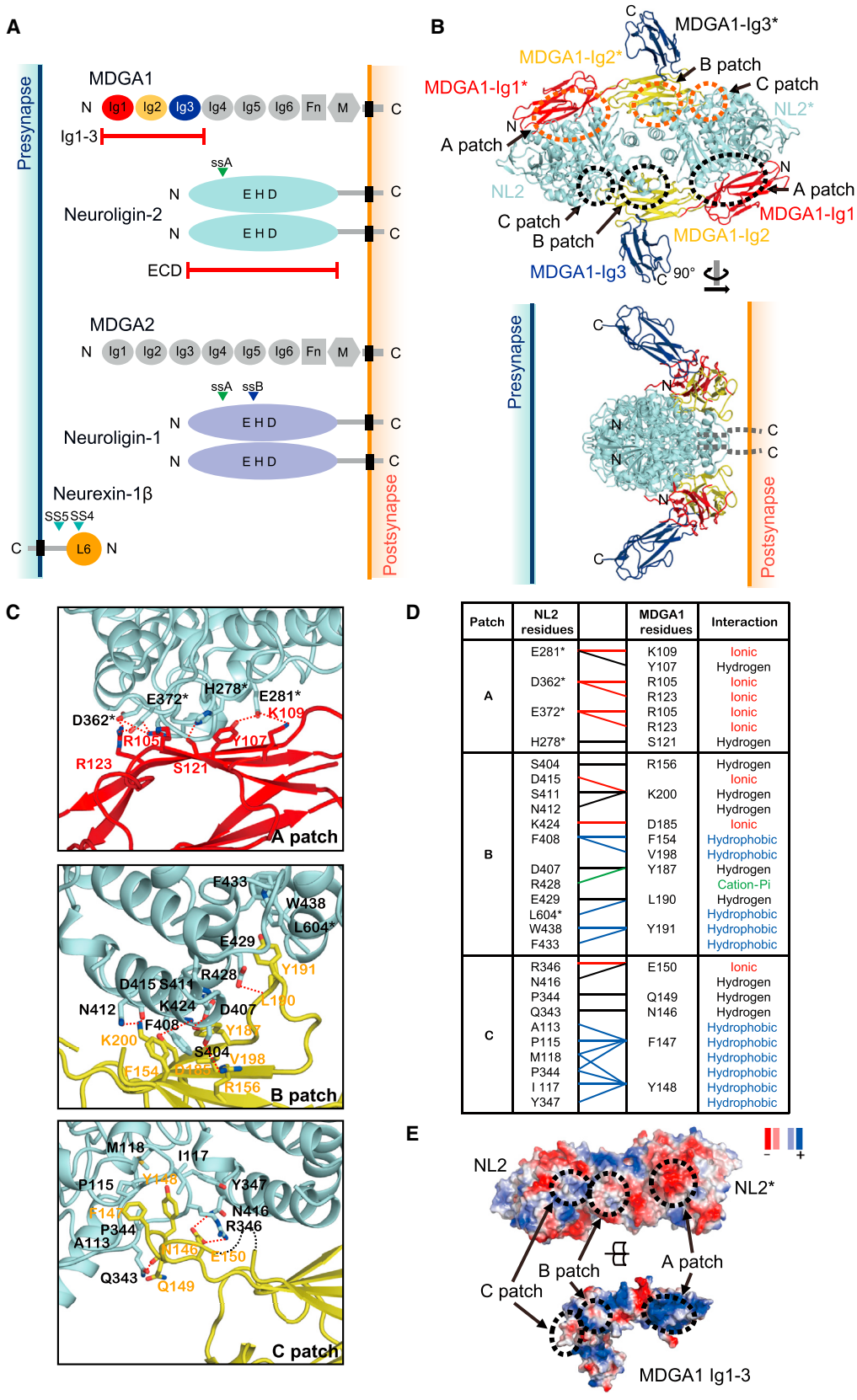

(legend on next page)

found that MDGA2 functions as a specificity factor at inhibitory synapses to negatively regulate selective NL2 signaling machinery (Loh et al., 2016). In contrast, another study using *Mdga2* knockout mice, displaying a variety of autism-like behaviors resulting from intrahemispheric functional connectivity alteration, suggested that MDGA2 primarily acts as a negative regulator of excitatory synapse development, in particular through modulation of NL1 function (Connor et al., 2016). The discrepancies between these findings, as well as the mechanism by which MDGA1 inhibits the ability of NL2 to modulate inhibitory synapse development at the molecular level, remain unclear.

Here, we determined the crystal structure of a minimal complex of NL2 and MDGA1 (NL2 EHD/MDGA1 Ig1-3) and investigated the interactions between NLs and MDGAs. Our data from the comprehensive analysis suggest that MDGA1 employs a specific mechanism to suppress NL2-mediated inhibitory synapse organization by disrupting *trans*-synaptic NL2-Nrx adhesion but may not suppress NL1-mediated excitatory synapse organization.

RESULTS

Overall Structure of the Human NL2/MDGA1 Complex

To investigate the molecular mechanism underlying the interaction between NL2 and MDGA1, we determined the crystal structure at 3.1 Å resolution of an extracellular domain complex of human NL2 (EHD, esterase homology domain) and the human MDGA1 Ig1-3, shown to be the minimal NL2-binding domain (Lee et al., 2013) (Figure 1A). We initially crystallized a complex of wild-type (WT) NL2 with MDGA1 Ig1-3 but did not obtain a diffractive crystal. Because mass spectroscopy analysis identified Asn98 as a major N-glycosylated residue in NL2 (Figure S1B), it was mutated to Gln (N98Q) to prevent NL2 N-glycosylation. This resulted in the successful crystallization of the NL2/MDGA1 Ig1-3 complex and determination of its structure (Figure 1). Although N98Q was a critical interface for the crystal packing of NL2/MDGA1 Ig1-3 complex, it was not involved in the interaction between NL2 and MDGA1 (Figure S1C). NL2 and MDGA1 Ig1-3 formed a heterodimeric complex with 1:1 stoichiometry in an asymmetric unit (Figure S1A). Of the three Ig domains of MDGA1 having L-shaped configuration, the Ig2 domain primarily mediates interactions with NL2 (Figure S1A). Because NLs are constitutively present as dimers (Poulopoulos et al., 2012), we examined the multimeric status of the NL2/MDGA1 Ig1-3 complex used for crystallization by performing size-exclusion chromatography. The results showed that this complex had a molecular weight of ~220 kDa (Figure S1D), indicating that the NL2/MDGA1 Ig1-3 complex formed a tightly associated heterotetramer with 2:2 stoichiometry in solution. Thus, we imposed C2 crystallographic symmetric operation to generate the biological assembly of NL2/MDGA1 Ig1-3 complex (heterotetramer with 2:2 stoichiometry) (Figure 1B; Figure S1C). This heterotetrameric NL2/MDGA1 Ig1-3 complex enabled the identification of additional interactions between MDGA1 Ig1 and the symmetric mate of NL2 (indicated as NL2*) (Figure 1B). Hereinafter, an asterisk will denote domains or residues in the symmetric mate of the NL2/MDGA1 Ig1-3 complex.

Binding Interfaces in the NL2/MDGA1 Complex

The binding interfaces between NL2 and MDGA1 Ig1-3 could be divided into three distinct regions, termed A, B, and C patches (Figures 1B–1D; Figure S2). A patch's interactions, with a buried surface area of 754 $Å^2$, are mainly mediated by long-range electrostatic charge interactions between the MDGA1 Ig1 domain and NL2* (Figures 1C, top, 1D, and 1E). Residues R105, Y107, K109, S121, and R123 on the βE–βF of the MDGA1 Ig1 domain form ionic or hydrogen bonds with residues H278*, E281*, D362*, and E372* on the NL2* loop connecting α8 and β10 and the loop flanking α12 of NL2* (Figures 1C, top, and 1D). The MDGA1 Ig2 domain and NL2 contribute to the B and C patch interactions, with a total buried surface area of 1,151 $Å^2$. In the B patch, βB, βD, and βE of the MDGA1 Ig2 domain surround α14–α15 of NL2 through electrostatic and hydrophobic interactions (Figures 1C, middle, and 1D). Multiple electrostatic interactions and hydrogen bonds are mediated by residues R156, D185, Y187, and K200 of the MDGA1 Ig2 domain and S404, D407, S411, N412, D415, K424, and R428 of NL2, surrounding the hydrophobic interactions between residues F154 on βB and V198 on βE of the MDGA1 Ig2 domain and NL2 residue F408. Intriguingly, L190 and Y191 on the loop connecting βD and βE of the MDGA1 Ig2 domain are located at the cleft of the NL2 dimeric interface and hydrophobically interact with W438 on α15 of NL2 and L604* on α21 of NL2* (Figures 1C, middle, and 1D). In the C patch, F147 and Y148 on the loop between βA and βB of MDGA1 Ig2 bind to the hydrophobic pocket of NL2, composed of residues A113, P115, I117, M118, P344,

Figure 1. Crystal Structure of Heterotetrameric NL2/MDGA1 Ig1-3 Complex

(A) Schematic showing the domain structures of the MDGA, neuroligin family (NL1 and NL2), and neurexin-1β (Nrx1β). Abbreviations: Ig, Ig-like domain; Fn, fibronectin type III repeat; M, single meprin/A5 protein/receptor protein tyrosine phosphatase mu (MAM) domain; EHD, esterase homology domain; ECD, extracellular domain; ss, alternative splicing site; N, N-terminal; C, C-terminal.

(B) Overview of the heterotetrameric NL2/MDGA1 Ig1-3 complex. The Ig1, Ig2, and Ig3 domains in MDGA1 Ig1-3 and NL2 are colored red, yellow, blue, and cyan, respectively. The A, B, and C patches of the interacting regions are indicated by dashed circles. The NL2/MDGA1 Ig1-3 dimer complex is generated by C2 crystallographic symmetric operation. Asterisks (NL2*/MDGA-Ig1*, Ig2*, and Ig3*) denote the symmetric mate of the NL2/MDGA1 Ig1-3 complex in the neighboring asymmetric unit.

(C) Close-up view of the A, B, and C binding patches. The residues involved in the interactions are displayed as sticks and labeled. Hydrogen bonds and electrostatic interactions are indicated by dashed red lines. The connectivity of the disordered flexible loop between βA and βB in MDGA1 Ig2 (amino acids 140~145) is indicated by the dashed black lines.

(D) Key amino acid residues of the A, B, and C patches involved in complex formation.

(E) Electrostatic potential of MDGA1 Ig1-3 and NL2, as calculated by the Poisson-Boltzmann equation in PyMOL. The structures are shown as open-book views and surface representations, with color maps reflecting electrostatic properties (blue, positively charged; red, negatively charged). The interacting patches are highlighted by a dashed black circle.

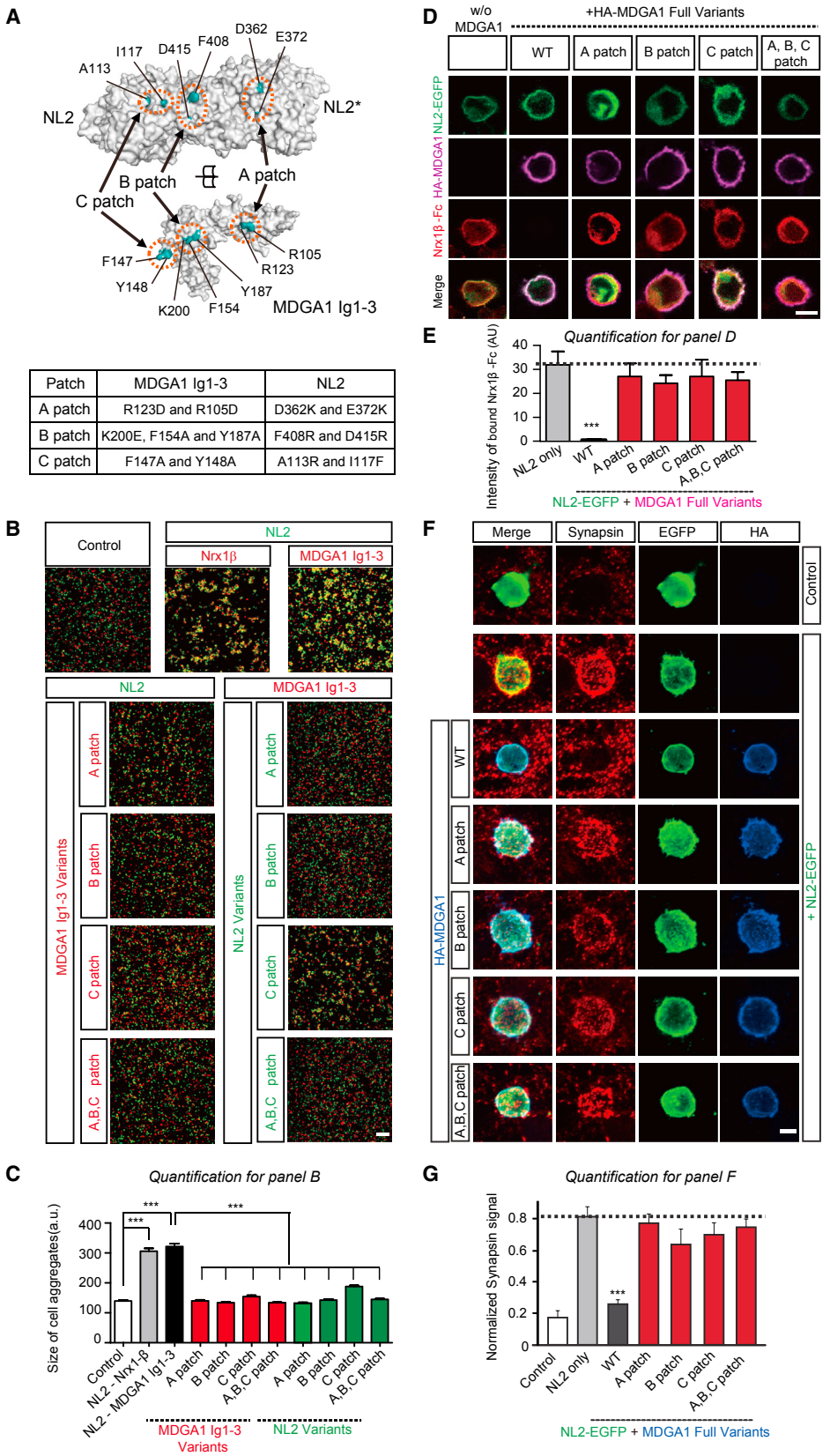

Patch	MDGA1 Ig1-3	NL2
A patch	R123D and R105D	D362K and E372K
B patch	K200E, F154A and Y187A	F408R and D415R
C patch	F147A and Y148A	A113R and I117F

(legend on next page)

and Y347 (Figures 1C, bottom, and 1D). These hydrophobic interactions are stabilized by neighboring hydrogen bonds and electrostatic interactions between residues N146, Q149, and E150 on the MDGA1 Ig2 domain and residues Q343, R346, and N416 on NL2.

Critical MDGA1 Residues Involved in NL2 Binding and NL2-Mediated Synaptogenic Activity

Based on the structural information of the heterotetrameric NL2/MDGA1 Ig1-3 complex, we designed a series of NL2 and MDGA1 Ig1-3 mutants that we predicted would not interact (Figure 2A). To identify the significance of each interaction patch in MDGA1 Ig1-3, we introduced specific point mutations in hemagglutinin (HA)-tagged pDisplay expression vectors encoding MDGA1 Ig1-3 (pDis-HA-MDGA1 Ig1-3-PDGFR TM). MDGA1 R105D and R123D mutants were designed to disrupt charge interactions in the A patch; F154A, Y187A, and K200E mutants to disrupt hydrophobic and ionic interactions in the B patch; and F147A and Y148A mutants to disrupt hydrophobic interactions in the C patch (Figure 2A). We then performed cell adhesion assays, where one group of L cells co-expressing EGFP and WT NL2 was mixed with a second group co-expressing DsRed and each MDGA1 Ig1-3 mutant (Figures 2B, left, and 2C). We found that all MDGA1 Ig1-3 mutants were defective in NL2 binding, suggesting that these highly conserved residues in the A, B, and C patches of MDGA1 are required for stable NL2/MDGA1 interactions (Figure S2). We also examined the interactions between NL2 mutants and WT MDGA1 in similar cell adhesion assays (Figure 2A). We found that the binding of these NL2 mutants to MDGA1 was significantly reduced, although the extent of reduction differed slightly among them (Figures 2B, right, and 2C).

Although these cell adhesion assays showed the significance of the three interacting interfaces on NL2 and MDGA1, these interactions were in a *trans*-configuration. Because MDGA1 and NL2 were previously proposed to interact in a *cis* manner on dendrite surfaces (Lee et al., 2013; Pettem et al., 2013), we also analyzed their *cis*-interactions by monitoring Nrx1β binding to the surfaces of HEK293T cells co-expressing EGFP-fused WT NL2 and HA-tagged WT or mutant MDGA1. We confirmed that MDGA1 variants (WT and mutants) were highly expressed on cell surfaces with proper folding and were co-localized with WT NL2 on the membranes of these transfected HEK293T cells (Figure 2D; Figure S1E). Cy5-labeled Nrx1β-Fc was unable to bind NL2-EGFP on the surfaces of cells also expressing WT HA-MDGA1, possibly due to the already stable association between NL2-EGFP and WT HA-MDGA1 (Figures 2D and 2E; Figure S1F). In contrast, Cy5-labeled Nrx1β-Fc interacted strongly with NL2-EGFP on the surfaces of cells expressing NL2-EGFP with or without the indicated HA-MDGA1 mutants (Figures 2D and 2E). Therefore, the *cis*-interaction of NL2 with MDGA1 may be mediated via all binding interfaces, which inhibits Nrx1β binding to NL2.

Next, we investigated whether MDGA1 mutants defective in NL2 binding are also defective in negatively regulating NL2-induced synaptogenic activity in heterologous synapse-formation assays. We found that all examined MDGA1 mutants defective in NL2 binding were unable to inhibit NL2-mediated synaptogenic activity (Figures 2F and 2G). Taken together, these findings indicate that the conserved residues in the A, B, and C patches of MDGA1 are crucial for NL2 binding and the negative regulation of NL2-mediated synaptogenic activity.

Comparison of the Binding Interfaces of NL2/MDGA1 and NL1/Nrx1β Complexes

Superposition of human NL2 in the NL2/MDGA1 Ig1-3 complex with mouse apo-NL2 (PDB: 3BL8) (Koehnke et al., 2008) resulted in root-mean-square deviation (RMSD) of 0.87 Å over 521 Cα atoms, indicating that the structures of human and mouse NL2 are well conserved and that there was no substantial change in NL2 backbone structure upon binding to MDGA1 (Figure S3A). Although the splice site A (ssA) in the NL2/MDGA1 Ig1-3 complex was disordered, the ssA structure in the NL1/Nrx1β complex (PDB: 3VKF) (Tanaka et al., 2012) suggested that the NL2 ssA positioned opposite the NL2/MDGA1 interface did not directly affect MDGA1 binding (Figure 3A, right; Figure S3B).

We next compared the structures and binding interfaces of the NL2/MDGA1 Ig1-3 and NL1/Nrx1β (PDB: 3VKF) complexes to examine how MDGA1 modulates the interaction of NL2 with Nrx1β. Although both MDGA1 and Nrx1β bound to NLs with a

Figure 2. Residues Critical for MDGA1 Binding to NL2 and Inhibition of NL2-Mediated Synaptogenic Activity

(A) Open-book view showing the interacting interfaces of the NL2/MDGA1 Ig1-3 complex. The orientations of NL2 and MDGA1 Ig1-3 are identical to those in Figure 1E. The amino acid residues mutated for functional analyses are labeled and shown in blue; the mutated residues in the A, B, and C patches are shown in the table.

(B and C) Representative images (B) and summary bar graphs (C) for cell adhesion assays. (B) Top: L cells expressing EGFP alone (Control) or co-expressing EGFP and NL2 wild-type (WT) were mixed with L cells expressing DsRed alone (control) or DsRed and Nrx1β or WT MDGA1 Ig1-3. Bottom left: L cells co-expressing EGFP and WT NL2 were mixed with L cells co-expressing DsRed and MDGA1 Ig1-3 mutants. Bottom right: L cells co-expressing DsRed and WT MDGA1 Ig1-3 were mixed with L cells co-expressing EGFP and NL2 mutants. Scale bar for all images, 100 μm.

(D and E) Representative image (D) and summary bar graphs (E) for binding assays of Cy5-labeled Nrx1β-Fc onto the surfaces of HEK293T cells. HEK293T cells co-expressing NL2-EGFP and hemagglutinin (HA)-tagged MDGA1 full variants (WT and mutants) were incubated with Cy5-labeled Nrx1β-Fc, with binding of the latter monitored by Cy5 fluorescence signaling. NL2-EGFP and HA-tagged MDGA1-variants were analyzed by immunostaining with antibodies against EGFP (green) and HA (purple). Nrx1β-Fc binding was quantified as the ratio of Cy5-labeled Nrx1β-Fc to EGFP fluorescence signals. Scale bar for all images, 10 μm.

(F and G) Representative images (F) and summary bar graphs (G) for heterologous synapse-formation assays. HEK293T cells co-transfected with NL2-EGFP and HA-tagged MDGA1 variants (WT and mutants) were co-cultured with hippocampal cultured neurons. HEK293T cells transfected with EGFP alone (Control) were the negative control. After 24 hr, co-cultured cells were immunostained with antibodies against synapsin (red), EGFP (green), and HA (blue). Heterologous synapse-formation assays were quantified as the ratio of synapsin to EGFP fluorescence signals. Scale bar for all images, 10 μm.

In (E) and (G), the dashed line, corresponding to the control value, was set as baseline. In (C), (E), and (G), error bars represent the SEM from 12–22 cells in each of at least three independent experiments.

All data are shown as mean ± SEM, and statistical significance was assessed by the non-parametric Kruskal-Wallis test (***$p < 0.001$).

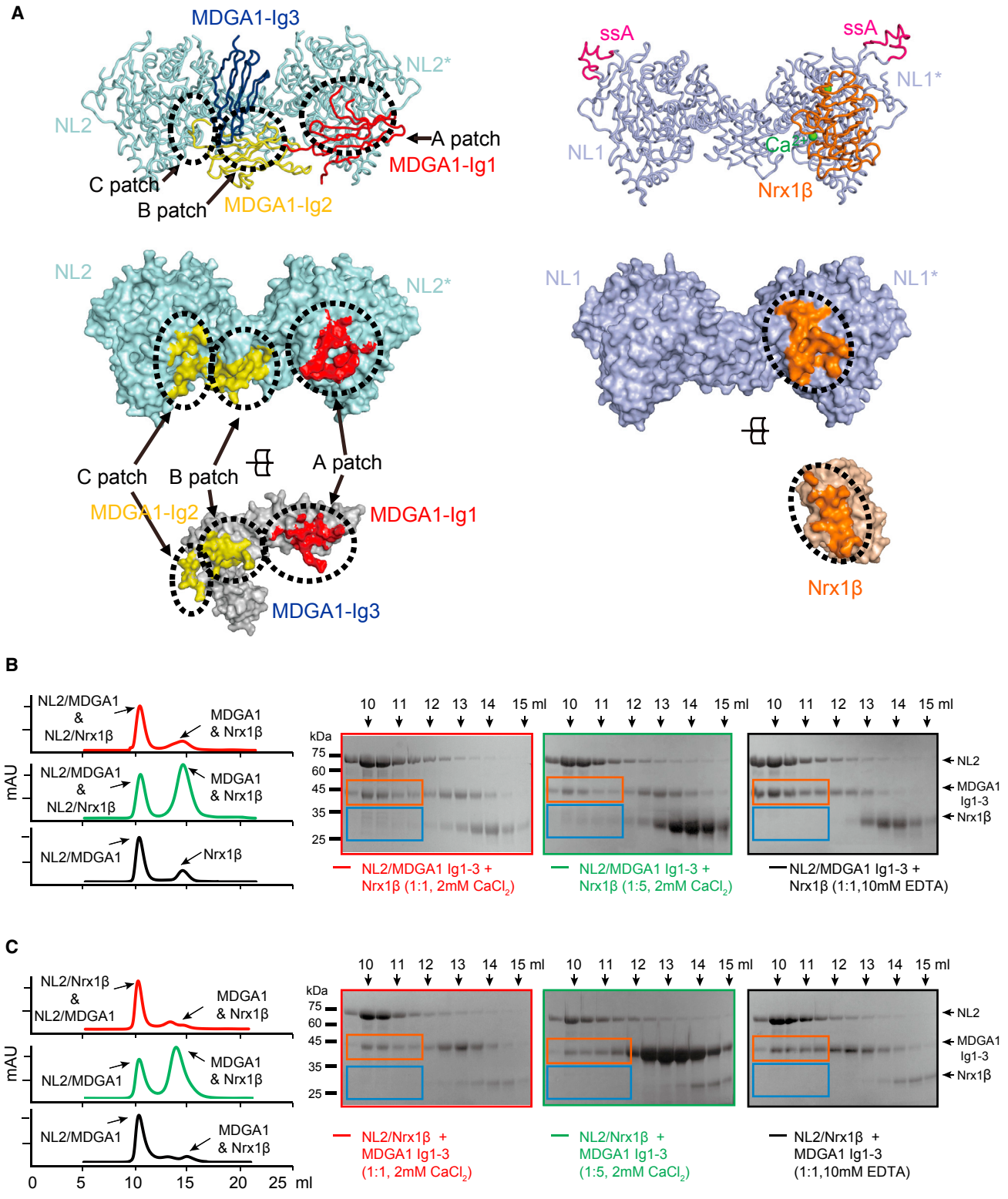

Figure 3. Comparison of Binding Interfaces for the NL2/MDGA1 and NL1/Nrx1β Complexes

(A) The NL2/MDGA1 Ig1-3 and NL1/Nrx1β complexes, with NL2 and NL1 in the same orientation, are presented as ribbons (top) and surfaces (bottom). The color scheme of the NL2/MDGA1 Ig1-3 complex (top left) is identical to the color scheme in Figure 1B. The interacting regions, divided into A, B, and C patches, are indicated by the dotted black circles. NL1, NL1 splice site A (ssA), Nrx1β, and Ca^{2+} ions of the NL1/ Nrx1β complex are colored purple, magenta, orange, and

(legend continued on next page)

2:2 symmetrical arrangement, each MDGA1 Ig1-2 domain spanned an NL2 dimer, resulting in a larger interaction interface (~2,000 Å^2 for the A, B, and C patches) than that of the NL1/Nrx1β complex (585 Å^2) (Figure 3A). Interestingly, the NL2 region binding to MDGA1 Ig1 largely overlapped with that binding to Nrx1β. In contrast to the NL1/Nrx1β complex, however, the NL2/MDGA1 Ig1 complex did not require Ca^{2+}.

Competition between MDGA1 and Nrx1β for NL2 Binding in the Presence of Ca^{2+}

Because MDGA1 Ig1 and Nrx1β bind to the same region of NL2, we investigated whether MDGA1 competes with Nrx1β for NL2 binding. The NL2/MDGA1 Ig1-3 complex and Nrx1β were mixed at a molar ratio of 1:1 or 1:5 in the presence of 2 mM $CaCl_2$ or 10 mM EDTA and analyzed by size-exclusion chromatography. Although the gel-filtration profiles of NL2/MDGA1 Ig1-3 complex (~220 kDa) and NL2/Nrx1β complex (~200 kDa) are indistinguishable due to limited resolution, SDS-PAGE analysis of each eluted fraction showed that the NL2/MDGA1 Ig1-3 complex remains intact in the presence of EDTA, whereas the amount of Nrx1β bound to NL2 in the presence of Ca^{2+} is slightly increased at a 5-fold molar excess of Nrx1β (Figure 3B, blue box). Therefore, Nrx1β can compete with MDGA1 for NL2 binding, and Ca^{2+} may be required for this competition. We next incubated the NL2/Nrx1β complex with MDGA1 Ig1-3. We found that EDTA induced complete dissociation of Nrx1β from NL2 and that MDGA1 bound to NL2 (Figure 3C, right). Interestingly, when MDGA1 was incubated with the NL2/Nrx1β complex at a 1:1 molar ratio in the presence of Ca^{2+}, most of Nrx1β was displaced by MDGA1, yielding stable NL2/MDGA1 Ig1-3 complex (Figure 3C, left). When 5-fold molar excess of MDGA1 was mixed with the NL2/Nrx1β complex, the NL2/Nrx1β complex was completely converted to the NL2/MDGA1 Ig1-3 complex (Figure 3C, middle). These results suggest that MDGA1 and Nrx1β compete for NL2 binding, although MDGA1 binding is favored, probably due to its wider interface for NL2 binding.

Binding Kinetics of MDGA1 and Nrx1β with NLs

The binding affinities of MDGA1 and Nrx1β with NL2 were directly compared in the presence of Ca^{2+} by biolayer light interferometry. The pertinent experiments showed that, relative to MDGA1, Nrx1β had slower on-rates and faster off-rates to NL2. Accordingly, the binding affinity of Nrx1β to NL2 (K_{D1} = 122 nM, K_{D2} = 5.8 μM) was much lower than that of MDGA1 to NL2 (K_{D1} = 0.4 nM, K_{D2} = 11 nM) (Figure 4A, top; Table S2), a finding consistent with our competitive binding analysis (Figures 3B and 3C). These results suggest that if similar concentrations of MDGA1 and Nrx1β are present at synaptic clefts, MDGA1 may dominantly capture NL2 and suppress NL2-mediated synaptogenic activity by blocking the access of NL2 to Nrx1β.

Previous studies have shown that both MDGA1 and MDGA2 bind to NL2 and that MDGA2 binds to both NL1 and NL2 (Connor et al., 2016; Lee et al., 2013; Pettem et al., 2013). Therefore, we next analyzed the binding affinities of MDGA1 and MDGA2 to NL1 and NL2 to assess the binding specificity of each pair. These analyses revealed that MDGA1 and MDGA2 robustly bound to NL1 and NL2 with similar binding affinities in vitro, although MDGA1 had a slightly higher binding affinity than MDGA2 to NLs (Figure 4A; Table S2). In addition, size-exclusion chromatography consistently showed that both MDGAs can form stable complexes with both NLs (Figure S3C). Furthermore, the sequence alignment of MDGAs demonstrated that the key residues of MDGA1 for NL2 binding are highly conserved in MDGA2 (Figure S2). These indicate that MDGA1 and MDGA2 can non-discriminately interact with NL1 and NL2, at least in vitro.

Although both NLs contain a common splice site at position A (ssA), NL1 can have an additional one at position B (ssB) (Chih et al., 2006). Nrx1β can bind to NL1 regardless of the presence of ssB, but this splice site lowers the Nrx1β-binding affinity ~2-fold, probably due to its proximity to the Nrx1β-binding surface (Comoletti et al., 2006; Koehnke et al., 2010). Intriguingly, the MDGA1-binding site is also located close to the ssB of NL1 (Figure S3B). We, therefore, analyzed the effects of ssB on the interaction of MDGAs with NL1 by comparing the binding kinetics of MDGAs to two NL1 splice variants, NL1AB (presence of ssB) and NL1A (lack of ssB). Interestingly, we observed no significant differences in the K_D, kon, and kdis of MDGAs to NL1AB and NL1A (Figure 4A, middle and bottom; Table S2), suggesting that the splice insert ssB of NL1 does not influence the interaction between MDGAs and NL1.

Because our results differed from those of previous studies on the interactions between MDGAs and NLs (Lee et al., 2013; Pettem et al., 2013; Connor et al., 2016), we performed pull-down assays by incubating Fc-fusion proteins of rat NLs (rNL1-Fc and rNL2-Fc) and Fc (negative control) with cell lysates of HEK293T cells expressing HA-tagged MDGA expression vectors (HA-MDGA1 and HA-MDGA2) and a FLAG-tagged Nrx1β construct (positive control). Both rNL1-Fc and rNL2-Fc captured both MDGAs (Figure 4B; Figure S4C), consistent with our binding affinity results (Figure 4A; Table S2). However, pull-down assays using detergent-solubilized mouse brain membrane fractions showed enrichment of MDGA1 by NL2, but not NL1 (Figure 4C; see Figure S4 for our in-house MDGA1 antibody characterization). Moreover, parallel pull-down assays showed selective enrichment of NL2, but not NL1, PSD-95, or TrkC, in MDGA1-bound fractions (Figure 4D). These experiments unequivocally demonstrate that, although the mechanisms by which MDGAs

green, respectively (top right, PDB: 3VKF). The surface representations are open-book views showing the interacting interfaces of the NL2/MDGA1 Ig1-3 and NL1/ Nrx1β complexes (bottom).

(B and C) Size-exclusion chromatography analysis of the competition of MDGA1 Ig1-3 with Nrx1β for NL2 binding. The NL2/MDGA1 Ig1-3 complex and Nrx1β were mixed at molar ratios of 1:1 (red peak) and 1:5 (green peak) in the presence of 2 mM $CaCl_2$ or at a 1:1 molar ratio in the presence of 10 mM EDTA (black peak), followed by size-exclusion chromatography (B). The NL2/Nrx1β complex was mixed with MDGA1 Ig1-3 at molar ratios of 1:1 (red peak) and 1:5 (green peak) in the presence of 2 mM $CaCl_2$ or at a 1:1 molar ratio in the presence of 10 mM EDTA (black peak), followed by size-exclusion chromatography (C). Effluent fractions were analyzed by SDS-PAGE and Coomassie blue staining (right). The retention volumes are indicated above the SDS-PAGE images. MDGA1 Ig1-3 and Nrx1β bound to NL2 are indicated by the orange and blue boxes, respectively.

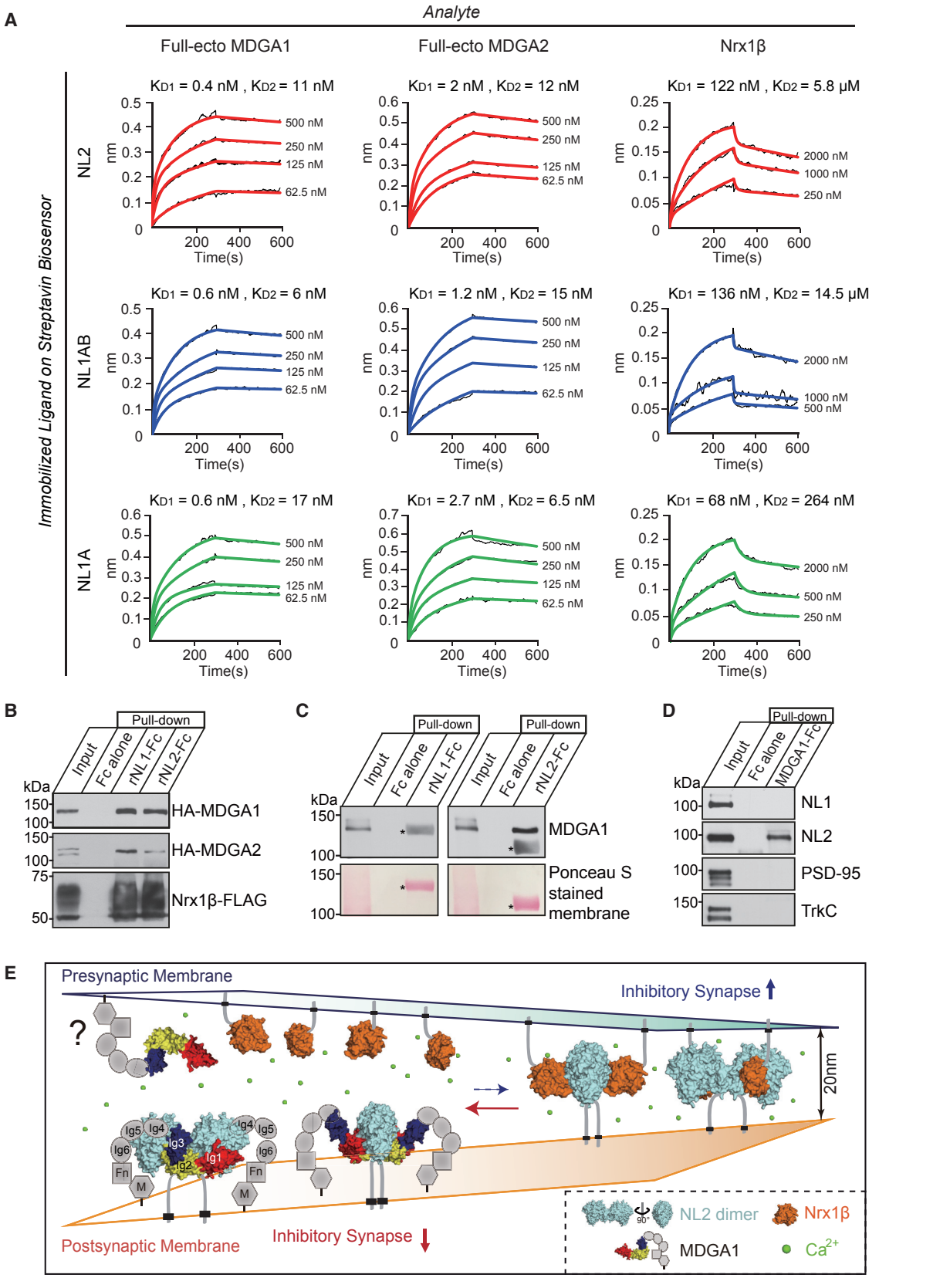

(legend on next page)

bind to NLs are overall identical, unidentified processes may dictate the selective association of MDGA1 with NL2, but not NL1, in vivo.

DISCUSSION

The *trans*-synaptic complex formation of Nrx and NLs is a central event in the specification and maturation, but not the initial formation, of both excitatory and inhibitory synapses (Südhof, 2008). MDGAs, which inhibit the formation of NLs-Nrx1β complexes by *cis*-interactions with NLs, have been found to be important regulators of synaptic adhesion pathways at both excitatory and inhibitory synapses (Connor et al., 2016; Lee et al., 2013; Loh et al., 2016; Pettem et al., 2013).

In this study, we determined the crystal structure of the NL2/MDGA1 complex (heterotetramer with 2:2 stoichiometry) (Figure 1). We found that, of the first three Ig-domains of MDGA1, only Ig1 and Ig2 are involved in interactions between MDGA1 and NL2 via three distinctive interaction patches, which are equally crucial for their interactions (Figure 2). Notably, we observed that MDGA1 and NL2 form an intercellular adhesion complex, probably induced by *trans*-configuration-mediated interactions. Because axons have been reported to contain a subset of MDGA1 recombinant proteins (Pettem et al., 2013), NL2 likely binds to MDGA1 in both *cis*- and *trans*-configurations in a context-dependent manner associated with the presence of MDGA1 proteins at either presynaptic or postsynaptic membranes. However, it was difficult to determine whether these protein interactions are *cis*- or *trans*-cellular. To address this possibility, the ultrastructural localization of MDGAs at synapses and the structures of the complete ecto-domains of MDGAs should be determined.

Our structural comparisons and comprehensive biochemical analysis indicate that MDGA1 and Nrxs may compete in binding to NL2 at the inhibitory synaptic sites (Figure 3). The Ig1 domain of MDGA1 (A patch) binds the Nrx1β-binding interface of NL2, but MDGA1 binding to NL2 is also mediated by additional interaction interface in the Ig2 domain of MDGA1 (B and C patches). These larger interaction interfaces of the MDGA1/NL2 complex are in agreement with the 30- to ~60-fold higher binding affinity of MDGA1 than Nrx1β toward NLs. In addition, we found that MDGA1 binding to NL2 is independent of Ca^{2+}, an ion required for the binding of NL2 to Nrx1β. Therefore, NL-mediated synapse development is likely to be finely modulated by the concentrations of local MDGA proteins and Ca^{2+}. The levels of MDGA proteins may be regulated by specific patterns of synaptic activity, which are causally linked to activity-dependent synapse refinement and elimination involving NLs/Nrxs *trans*-synaptic adhesion complexes.

MDGA1 and MDGA2 were shown to interact with NL2, but not NL1 or NL3, although one study reported that MDGA2 binds to both NLs (Connor et al., 2016; Lee et al., 2013; Pettem et al., 2013). Thus, it was necessary to examine whether the binding specificities of MDGAs and NLs are determined by specific mechanisms. The biochemical analysis in the current study clearly demonstrated that both NLs bind with comparative affinity to MDGA1 and MDGA2, although MDGA1 has slightly higher binding affinities to NLs than MDGA2 (Figure 4). This is consistent with the structural and sequence conservation of key residues involved in their binding interface with NL1 and NL2. Intriguingly, pull-down assays showed that MDGA1 selectively forms complexes with NL2, but not with NL1, suggesting the existence of a specific mechanism to inhibit the formation of MDGA1/NL1 complexes. Although the precise location of endogenous MDGA proteins has not yet been determined due to a lack of sufficiently suitable antibodies for immunohistochemistry, experiments in cultured hippocampal neurons have shown that recombinant MDGA1 proteins localize to both excitatory and inhibitory synaptic sites, whereas recombinant MDGA2 proteins localize mainly to inhibitory synapse (Loh et al., 2016; Pettem et al., 2013). In contrast, *Mdga2*-KO mice showed increased surface AMPA receptor-mediated excitatory synaptic transmission and long-term synaptic plasticity (Connor et al., 2016). Moreover, overexpression of MDGA1 was found to specifically reduce inhibitory, but not excitatory, synaptic transmission in cultured cortical neurons (Lee et al., 2013). Thus, these data cannot be incorporated into a single unified model. Although a possibility that a subset of MDGA1 proteins may interact with NL1 at excitatory synapses cannot be excluded, unidentified processes may be also involved in the selective association of MDGA1 with only NL2. Further in-depth study, including functional analyses of *Mdga1*-KO mice and determination of the specific localization of endogenous MDGAs, is required to resolve these issues.

Similar to NLs and Nrxs, MDGAs have been implicated in autism spectrum disorders (ASDs) and other neurodevelopmental disorders. Intronic single nucleotide polymorphisms

Figure 4. Binding Kinetics of MDGAs with NLs

(A) Binding curves of MDGA1, MDGA2, and Nrx1β toward dimeric NL2, NL1AB, and NL1A at the indicated concentrations, starting at maximum concentrations of 500 nM for MDGAs and 2 μM for Nrx1β. Sensorgrams were obtained from an Octet RED96 instrument. Data points are shown in black, and the corresponding fits are shown in red (NL2), blue (NL1AB), and green (NL1A). K_D values were calculated from 2:1 global fitting.

(B) Pull-down assays in HEK293T cells expressing HA-MDGA1, HA-MDGA2, and Nrx1β−FLAG (positive control) using Fc, rNL1-Fc, and rNL2-Fc (input = 5% of total). The numbers on the left indicate molecular mass markers (kDa). Equivalent amounts of bound proteins were analyzed with the indicated antibodies.

(C and D) Pull-down assays in solubilized P14 mouse brain synaptosomes using rNLs-Fc (C) and MDGA1-Fc (D), with Fc as the negative control. Equivalent amounts of bound protein were analyzed using the antibodies against the proteins indicated on the right (input = 5% of total). Asterisks denote the positions of rNL1-Fc and rNL2-Fc fusion proteins used for the pull-down assays, as revealed by direct comparison of the bands in parallel Ponceau S-stained membranes (C, bottom).

(E) Model of MDGA1 action on NL2-mediated inhibitory synapse organization. Neuroligin-2 (NL2), an inhibitory synapse-specific postsynaptic organizer that forms a constitutive dimer (cyan), *trans*-synaptically interacts with presynaptic neurexins (orange) in a Ca^{2+} (green)-dependent manner. The local concentration of MDGA1 protein controls the state of NL2 in a manner that blocks physical access to presynaptic neurexins (left). When the MDGA1 level is lowered, NL2 binds to neurexins to specify inhibitory synapse development in a Ca^{2+}-dependent manner (right). A subset of MDGA1 localized in presynaptic neurons may mediate *trans*-synaptic adhesion interactions with postsynaptic NL2, although the physiological significance of presynaptic MDGA1 remains unclear.

(SNPs) of MDGA1 have been linked to schizophrenia and bipolar disorder (Kähler et al., 2008; Li et al., 2011). Four types of exonic deletions of the MDGA2 gene have been also found in patients with ASD (Bucan et al., 2009). These mutations may interfere with MDGA2 protein expression or truncate the MAM domain, resulting in the absence of the GPI anchor site and preventing MDGA2 from interacting with NL2 at the postsynaptic membrane. Thus, suppression of NL2/Nrxs synaptic adhesion pathways by MDGA1 (and MDGA2) may not always be detrimental to normal synapse development. Rather, fine-tuning of these critical synapse components can collectively contribute to a balance in excitation-to-inhibition ratio at various synapses and associated neural circuits.

In conclusion, our integrative investigations of MDGAs/NLs complexes provide a framework showing that MDGA1 functions as a negative regulator of inhibitory synapse development by directly inhibiting the binding of NL2 to Nrx1β (Figure 4E). These findings strengthen our current understanding of NL-Nrx synaptic adhesion pathways.

STAR★METHODS

Detailed methods are provided in the online version of this paper and include the following:

- KEY RESOURCES TABLE
- CONTACT FOR REAGENT AND RESOURCE SHARING
- EXPERIMENTAL MODEL AND SUBJECT DETAILS
  - Cell Culture
  - Rat Hippocampal Neuron Culture
- METHOD DETAILS
  - Proteins Expression and Purification
  - Glycosylation Site Analysis
  - Crystallization and Structural Determination
  - Cell Adhesion Assays
  - Cy5-Nrx1β-Fc Binding Assays on Cell Surfaces
  - Heterologous Synapse-Formation Assays
  - Size Exclusion Chromatography
  - Determination of Binding Kinetics
  - Generation of Polyclonal Antibody to MDGA1
  - Pull-Down Assays
- QUANTIFICATION AND STATISTICAL ANALYSIS
  - Cell Adhesion Assay
  - Nrx1β Binding Assays on Cell Surfaces
  - Heterologous Synapse-Formation Assays
- DATA AND SOFTWARE AVAILABILITY
  - Data Resources

SUPPLEMENTAL INFORMATION

Supplemental Information includes four figures and two tables and can be found with this article online at http://dx.doi.org/10.1016/j.neuron.2017.05.034.

AUTHOR CONTRIBUTIONS

Conceptualization, H.M.K. and J.K.; Methodology, H.M.K., J.K., J.-O.L., J.W.U., E.K., and H.J.A.; Investigation, H.M.K., J.A.K., D.K., S.Y.W., K.A.H., D.P., E.C., and N.Y.; Writing, H.M.K., J.K., J.A.K., D.K., S.Y.W., and H.J.A.; Funding Acquisition, H.M.K., J.K., D.K., and E.K.; Supervision, H.M.K., J.K., and J.-O.L.

ACKNOWLEDGMENTS

This work was supported by grants from the National Research Foundation of Korea (NRF-2015R1A2A2A01005533 to H.M.K. and 2016R1A2B2006821 to J.K.), the Institute for Basic Science (IBS) (IBS-R002-D1 to H.M.K., D.K., and E.K.), and the Intelligent Synthetic Biology Center of Global Frontier Project (2011-0031955). We would like to thank the staff of Y-Biologics for helping with the analysis of binding kinetics with the Octet RED96 system (ForteBio, Pall Life Sciences).

Received: April 9, 2017
Revised: May 9, 2017
Accepted: May 24, 2017
Published: June 21, 2017

REFERENCES

Adams, P.D., Grosse-Kunstleve, R.W., Hung, L.W., Ioerger, T.R., McCoy, A.J., Moriarty, N.W., Read, R.J., Sacchettini, J.C., Sauter, N.K., and Terwilliger, T.C. (2002). PHENIX: building new software for automated crystallographic structure determination. Acta Crystallogr. D Biol. Crystallogr. *58*, 1948–1954.

An, H.J., Tillinghast, J.S., Woodruff, D.L., Rocke, D.M., and Lebrilla, C.B. (2006). A new computer program (GlycoX) to determine simultaneously the glycosylation sites and oligosaccharide heterogeneity of glycoproteins. J. Proteome Res. *5*, 2800–2808.

Araç, D., Boucard, A.A., Ozkan, E., Strop, P., Newell, E., Südhof, T.C., and Brunger, A.T. (2007). Structures of neuroligin-1 and the neuroligin-1/neurexin-1 beta complex reveal specific protein-protein and protein-Ca2+ interactions. Neuron *56*, 992–1003.

Bemben, M.A., Shipman, S.L., Nicoll, R.A., and Roche, K.W. (2015). The cellular and molecular landscape of neuroligins. Trends Neurosci. *38*, 496–505.

Bucan, M., Abrahams, B.S., Wang, K., Glessner, J.T., Herman, E.I., Sonnenblick, L.I., Alvarez Retuerto, A.I., Imielinski, M., Hadley, D., Bradfield, J.P., et al. (2009). Genome-wide analyses of exonic copy number variants in a family-based study point to novel autism susceptibility genes. PLoS Genet. *5*, e1000536.

Chih, B., Gollan, L., and Scheiffele, P. (2006). Alternative splicing controls selective trans-synaptic interactions of the neuroligin-neurexin complex. Neuron *51*, 171–178.

Comoletti, D., Flynn, R.E., Boucard, A.A., Demeler, B., Schirf, V., Shi, J., Jennings, L.L., Newlin, H.R., Südhof, T.C., and Taylor, P. (2006). Gene selection, alternative splicing, and post-translational processing regulate neuroligin selectivity for beta-neurexins. Biochemistry *45*, 12816–12827.

Comoletti, D., Miller, M.T., Jeffries, C.M., Wilson, J., Demeler, B., Taylor, P., Trewhella, J., and Nakagawa, T. (2010). The macromolecular architecture of extracellular domain of alphaNRXN1: domain organization, flexibility, and insights into trans-synaptic disposition. Structure *18*, 1044–1053.

Compaan, D.M., Gonzalez, L.C., Tom, I., Loyet, K.M., Eaton, D., and Hymowitz, S.G. (2005). Attenuating lymphocyte activity: the crystal structure of the BTLA-HVEM complex. J. Biol. Chem. *280*, 39553–39561.

Connor, S.A., Ammendrup-Johnsen, I., Chan, A.W., Kishimoto, Y., Murayama, C., Kurihara, N., Tada, A., Ge, Y., Lu, H., Yan, R., et al. (2016). Altered cortical dynamics and cognitive function upon Haploinsufficiency of the autism-linked excitatory synaptic suppressor MDGA2. Neuron *91*, 1052–1068.

de la Torre-Ubieta, L., Won, H., Stein, J.L., and Geschwind, D.H. (2016). Advancing the understanding of autism disease mechanisms through genetics. Nat. Med. *22*, 345–361.

Emsley, P., and Cowtan, K. (2004). Coot: model-building tools for molecular graphics. Acta Crystallogr. D Biol. Crystallogr. *60*, 2126–2132.

Fabrichny, I.P., Leone, P., Sulzenbacher, G., Comoletti, D., Miller, M.T., Taylor, P., Bourne, Y., and Marchot, P. (2007). Structural analysis of the synaptic protein neuroligin and its beta-neurexin complex: determinants for folding and cell adhesion. Neuron *56*, 979–991.

Foadi, J., Aller, P., Alguel, Y., Cameron, A., Axford, D., Owen, R.L., Armour, W., Waterman, D.G., Iwata, S., and Evans, G. (2013). Clustering procedures for the optimal selection of data sets from multiple crystals in macromolecular crystallography. Acta Crystallogr. D Biol. Crystallogr. *69*, 1617–1632.

Han, K.A., Woo, D., Kim, S., Choii, G., Jeon, S., Won, S.Y., Kim, H.M., Heo, W.D., Um, J.W., and Ko, J. (2016). Neurotrophin-3 regulates synapse development by modulating TrkC-PTPσ synaptic adhesion and intracellular signaling pathways. J. Neurosci. *36*, 4816–4831.

Hua, S., Hu, C.Y., Kim, B.J., Totten, S.M., Oh, M.J., Yun, N., Nwosu, C.C., Yoo, J.S., Lebrilla, C.B., and An, H.J. (2013). Glyco-analytical multispecific proteolysis (Glyco-AMP): a simple method for detailed and quantitative Glycoproteomic characterization. J. Proteome Res. *12*, 4414–4423.

Kabsch, W. (2010). Xds. Acta Crystallogr. D Biol. Crystallogr. *66*, 125–132.

Kähler, A.K., Djurovic, S., Kulle, B., Jönsson, E.G., Agartz, I., Hall, H., Opjordsmoen, S., Jakobsen, K.D., Hansen, T., Melle, I., et al. (2008). Association analysis of schizophrenia on 18 genes involved in neuronal migration: MDGA1 as a new susceptibility gene. Am. J. Med. Genet. B. Neuropsychiatr. Genet. *147B*, 1089–1100.

Ko, J., Zhang, C., Arac, D., Boucard, A.A., Brunger, A.T., and Südhof, T.C. (2009). Neuroligin-1 performs neurexin-dependent and neurexin-independent functions in synapse validation. EMBO J. *28*, 3244–3255.

Koehnke, J., Jin, X., Budreck, E.C., Posy, S., Scheiffele, P., Honig, B., and Shapiro, L. (2008). Crystal structure of the extracellular cholinesterase-like domain from neuroligin-2. Proc. Natl. Acad. Sci. USA *105*, 1873–1878.

Koehnke, J., Katsamba, P.S., Ahlsen, G., Bahna, F., Vendome, J., Honig, B., Shapiro, L., and Jin, X. (2010). Splice form dependence of beta-neurexin/neuroligin binding interactions. Neuron *67*, 61–74.

Krueger, D.D., Tuffy, L.P., Papadopoulos, T., and Brose, N. (2012). The role of neurexins and neuroligins in the formation, maturation, and function of vertebrate synapses. Curr. Opin. Neurobiol. *22*, 412–422.

Lee, K., Kim, Y., Lee, S.J., Qiang, Y., Lee, D., Lee, H.W., Kim, H., Je, H.S., Südhof, T.C., and Ko, J. (2013). MDGAs interact selectively with neuroligin-2 but not other neuroligins to regulate inhibitory synapse development. Proc. Natl. Acad. Sci. USA *110*, 336–341.

Leone, P., Comoletti, D., Ferracci, G., Conrod, S., Garcia, S.U., Taylor, P., Bourne, Y., and Marchot, P. (2010). Structural insights into the exquisite selectivity of neurexin/neuroligin synaptic interactions. EMBO J. *29*, 2461–2471.

Li, J., Liu, J., Feng, G., Li, T., Zhao, Q., Li, Y., Hu, Z., Zheng, L., Zeng, Z., He, L., et al. (2011). The MDGA1 gene confers risk to schizophrenia and bipolar disorder. Schizophr. Res. *125*, 194–200.

Loh, K.H., Stawski, P.S., Draycott, A.S., Udeshi, N.D., Lehrman, E.K., Wilton, D.K., Svinkina, T., Deerinck, T.J., Ellisman, M.H., Stevens, B., et al. (2016). Proteomic analysis of unbounded cellular compartments: synaptic clefts. Cell *166*, 1295–1307.e21.

McCoy, A.J., Grosse-Kunstleve, R.W., Storoni, L.C., and Read, R.J. (2005). Likelihood-enhanced fast translation functions. Acta Crystallogr. D Biol. Crystallogr. *61*, 458–464.

Missler, M., Südhof, T.C., and Biederer, T. (2012). Synaptic cell adhesion. Cold Spring Harb. Perspect. Biol. *4*, a005694.

Otwinowski, Z., and Minor, W. (1997). Processing of X-ray diffraction data collected in oscillation mode. Methods Enzymol. *276*, 307–326.

Pettem, K.L., Yokomaku, D., Takahashi, H., Ge, Y., and Craig, A.M. (2013). Interaction between autism-linked MDGAs and neuroligins suppresses inhibitory synapse development. J. Cell Biol. *200*, 321–336.

Poulopoulos, A., Soykan, T., Tuffy, L.P., Hammer, M., Varoqueaux, F., and Brose, N. (2012). Homodimerization and isoform-specific heterodimerization of neuroligins. Biochem. J. *446*, 321–330.

Robert, X., and Gouet, P. (2014). Deciphering key features in protein structures with the new ENDscript server. Nucleic Acids Res. *42*, W320–W324.

Südhof, T.C. (2008). Neuroligins and neurexins link synaptic function to cognitive disease. Nature *455*, 903–911.

Tanaka, H., Miyazaki, N., Matoba, K., Nogi, T., Iwasaki, K., and Takagi, J. (2012). Higher-order architecture of cell adhesion mediated by polymorphic synaptic adhesion molecules neurexin and neuroligin. Cell Rep. *2*, 101–110.

Um, J.W., and Ko, J. (2013). LAR-RPTPs: synaptic adhesion molecules that shape synapse development. Trends Cell Biol. *23*, 465–475.

Um, J.W., Kim, K.H., Park, B.S., Choi, Y., Kim, D., Kim, C.Y., Kim, S.J., Kim, M., Ko, J.S., Lee, S.G., et al. (2014). Structural basis for LAR-RPTP/Slitrk complex-mediated synaptic adhesion. Nat. Commun. *5*, 5423.

Vink, T., Oudshoorn-Dickmann, M., Roza, M., Reitsma, J.J., and de Jong, R.N. (2014). A simple, robust and highly efficient transient expression system for producing antibodies. Methods *65*, 5–10.

STAR★METHODS

KEY RESOURCES TABLE

REAGENT or RESOURCE	SOURCE	IDENTIFIER
Antibodies		
Synapsin (rabbit polyclonal)	Han et al., 2016	JK014; RRID: AB_2651124
EGFP (goat polyclonal)	Rockland antibody & assays	Cat# 600-101-215; RRID: AB_218182
HA (mouse monoclonal)	Covance Research Products	Cat# MMS-101P; RRID: AB_2314672
Cy3 affiniPure Donkey Anti-Mouse IgG (H+L)	Jackson ImmunoResearch Laboratories	Cat# 715-165-150; RRID: AB_2340813
Alexa 647 AffiniPure Goat Anti-Rabbit IgG	Jackson ImmunoResearch Laboratories	Cat# 111-605-006; RRID: AB_2338073
Fluorescein (FITC) AffiniPure Donkey Anti-Guinea Pig IgG (H+L)	Jackson ImmunoResearch Laboratories	Cat# 706-095-148; RRID: AB_2340453
MDGA1 (rabbit polyclonal)	This study	JK030 (Abfrontier, AR15-PA0001); RRID: AB_2651125
Neuroligin-1 (mouse monoclonal)	UC Davis/NIH NeuroMab Facility	Cat# 73-160; RRID: AB_10671307
Neuroligin-2 (rabbit polyclonal)	Synaptic Systems	Cat# 129 202; RRID: AB_993011
PSD-95 (mouse monoclonal)	UC Davis/NIH NeuroMab Facility	Cat# 75-028; RRID: AB_2307331
TrkC (rabbit polyclonal)	Cell Signaling Technology	Cat# 3376S; RRID: AB_2155283
Chemicals, Peptides, and Recombinant Proteins		
Lipofectamin 2000	Invitrogen	Cat# 11668-019
Cy5 Maleimide Mono-Reactive Dye Pack	GE Healthcare Life Sciences	Cat# PA25031
Sulfo-NHS-LC-Biotin	Thermo Fisher Scientific	Cat# 21335
NL2 (42P–610N, N98Q)	This study	N/A
NL2 (15Q–610N)	This study	N/A
NL1 AB(46Q–634N)	This study	N/A
NL1 A (46Q–634N, -ssB: 295G–303K)	This study	N/A
MDGA1 Ig1-3 (19Q–330K)	This study	N/A
MDGA1 Ig1-6 (19Q–632A)	This study	N/A
Full-ecto MDGA1 (19Q–919K)	This study	N/A
MDGA2 Ig1-3 (20Q–332K)	This study	N/A
Full-ecto MDGA2 (20Q–914K)	This study	N/A
Nrx1β (51A–269S, -SS4)	This study	N/A
rNL1-Fc	Lee et al., 2013	N/A
rNL2-Fc	Lee et al., 2013	N/A
MDGA1 (Ig1-6)-Fc	This study	N/A
Critical Commercial Assays		
Superdex 200, 10/300 GL	GE Healthcare Life Sciences	Cat# 17517501
HiLoad 16/600 Superdex 200 pg	GE Healthcare Life Sciences	Cat# 28989335
Protein A Sepharose resin	GE Healthcare Life Sciences	Cat# 17-1279-01
IgG Sepharose resin	GE Healthcare Life Sciences	Cat# 17-0969-02
Bio-Gel P-6DG Gel	Bio-Rad	Cat# 1500738
Deposited Data		
Coordinate of NL2/MDGA1 Ig1-3 complex	This study	PDB: 5XEQ
Coordinate of NL1/Nrx1β complex	Araç et al., 2007	PDB: 3BIW
Coordinate of NL1/Nrx1β complex	Tanaka et al., 2012	PDB: 3VKF
Coordinate of mouse apo-NL2	Koehnke et al., 2008	PDB: 3BL8
human BTLA-HVEM complex	Compaan et al., 2005	PDB: 2AW2

(*Continued on next page*)

Continued

REAGENT or RESOURCE	SOURCE	IDENTIFIER
Experimental Models: Cell Lines		
High Five cells	Invitrogen	Cat# B85502
L cells	ATCC	Cat# CRL-2648
COS-7 cells	ATCC	Cat# CRL-1651
HEK293T cells	ATCC	Cat# CRL-3216
Recombinant DNA		
pDis-NL2-PDGFR TM WT (15Q–610N)	This study	N/A
pDis-NL2-PDGFR TM A patch mutant (15Q–610N), D362K, E372K	This study	N/A
pDis-NL2-PDGFR TM B patch mutant (15Q–610N), F408R, D415R	This study	N/A
pDis-NL2-PDGFR TM C patch mutant (15Q–610N), A113R, I117F	This study	N/A
pDis-NL2-PDGFR TM BC patch mutant (15Q–610N), F408R, D415R, A113R, I117F	This study	N/A
pDis-NL2-PDGFR TM ABC patch mutant (15Q–610N), F408R, D415R, A113R, I117F, D362K, D372K	This study	N/A
pDis-HA-MDGA1 Ig1-3-PDGFR TM WT (19Q–330K)	This study	N/A
pDis-HA-MDGA1 Ig1-3-PDGFR TM A patch mutant (19Q–330K), R123D, R105D	This study	N/A
pDis-HA-MDGA1 Ig1-3-PDGFR TM B patch mutant (19Q–330K), K200E, F154A, Y187A	This study	N/A
pDis-HA-MDGA1 Ig1-3-PDGFR TM C patch mutant (19Q–330K), F147A, Y148A	This study	N/A
pDis-HA-MDGA1 Ig1-3-PDGFR TM BC patch mutant (19Q–330K), K200E, F154A, Y187A, F147A, Y148A	This study	N/A
pDis-HA-MDGA1 Ig1-3-PDGFR TM ABC patch mutant (19Q–330K), R123D, R105D, K200E, F154A, Y187A, F147A, Y148A	This study	N/A
pDis-HA-MDGA1 full WT (19Q–919K)	This study	N/A
pDis-HA-MDGA1 full A patch mutant (19Q–919K) R123D, R105D	This study	N/A
pDis-HA-MDGA1 full B patch mutant (19Q–919K) K200E, F154A, Y187A	This study	N/A
pDis-HA-MDGA1 full C patch mutant (19Q–919K) F147A, Y148A	This study	N/A
pDis-HA-MDGA1 full BC patch mutant (19Q–919K) K200E, F154A, Y187A, F147A, Y148A	This study	N/A
pDis-HA-MDGA1 full ABC patch mutant (19Q–919K) R123D, R105D, K200E, F154A, Y187A, F147A, Y148A	This study	N/A
pEGFP-NL2-PDGFR TM (1M–610N)	This study	N/A
pEGFP	This study	N/A
pDsRed	This study	N/A
pcDNA3.1-NL2 (15Q–610N)-thrombin-Fc	This study	N/A
pcDNA3.1-NL1AB (46Q–634N)-thrombin-Fc	This study	N/A
pcDNA3.1-NL1A (46Q–634N, -ssB: 295G–303K)-thrombin-Fc	This study	N/A
pcDNA3.1-MDGA1 Ig1-3 (19Q∼330K)-thrombin-Fc	This study	N/A
pcDNA3.1-full-ecto MDGA1 (19Q∼919K)-thrombin-Fc	This study	N/A
pcDNA3.1-MDGA2 Ig1-3 (20Q∼332K)-thrombin-Fc	This study	N/A
pcDNA3.1-full-ecto MDGA2 (20Q∼914K)-thrombin-Fc	This study	N/A

(*Continued on next page*)

Continued

REAGENT or RESOURCE	SOURCE	IDENTIFIER
pcDNA3.1-Nrx1β (51A–269S, -SS4)-thrombin-Fc	This study	N/A
pcDNA3.1-Nrx1β (51A∼269S, -SS4)-Fc(S396C in Fc domain)	This study	N/A
pAcGP67A-NL2 (42P–610N, N98Q)-thrombin-Fc	This study	N/A
pAcGP67A-NL2 (15Q–610N)-thrombin-Fc	This study	N/A
pAcGP67A-NL2 (15Q–610N)	This study	N/A
pAcGP67A-MDGA1 Ig1-3 (19Q∼330K)-thrombin-Fc	This study	N/A
pAcGP67A-MDGA1 Ig1-6 (19Q∼632A)-thrombin-Fc	This study	N/A
pAcGP67A-Nrx1β (51A–269S, -SS4)-thrombin-Fc	This study	N/A
pCMV5-rNL1-Fc (rat 1–636)	Lee et al., 2013	N/A
pCMV5-rNL2-Fc (rat 1–612)	Lee et al., 2013	N/A
pCMV5-Fc	Lee et al., 2013	N/A
pGW1-HA-MDGA1	Lee et al., 2013	N/A
pGW1-HA-MDGA2	Lee et al., 2013	N/A
pCAG-FLAG-Nrx1β (-SS4)	Michisuke Yuzaki (Keio University)	N/A
Software and Algorithms		
PyMOL	Molecular Graphics System	https://www.pymol.org/
COOT	Emsley and Cowtan, 2004	http://www2.mrc-lmb.cam.ac.uk/personal/pemsley/coot/
HKL2000	Otwinowski and Minor, 1997	http://www.hkl-xray.com/
PHENIX	Adams et al., 2002	https://www.phenix-online.org/
XDS	Kabsch, 2010	http://xds.mpimf-heidelberg.mpg.de/
BLEND	Foadi et al., 2013	N/A
MetaMorph	Molecular Devices	N/A
ImageJ	NIH	https://imagej.nih.gov/ij/
Prism5	GraphPad	http://www.graphpad.com
ESPript	Robert and Gouet, 2014	http://espript.ibcp.fr/ESPript/ESPript/
PHASER	McCoy et al., 2005	http://www.phaser.cimr.cam.ac.uk/index.php/Phaser_Crystallographic_Software
Other		
Streptavidin (SA) Biosensors	Forte Bio	18-5021

CONTACT FOR REAGENT AND RESOURCE SHARING

Further information and requests for reagents may be directed to the Lead Contact Ho Min Kim (hm_kim@kaist.ac.kr).

EXPERIMENTAL MODEL AND SUBJECT DETAILS

Cell Culture

High Five cells were cultured at 28°C in Sf-900 II SFM medium (GIBCO) supplemented with 1% Antibiotic-Antimycotic (GIBCO). COS-7, HEK293T and L cells were cultured at 37°C in Dulbecco's Modified Eagle's Medium (DMEM, Welgene) supplemented with 10% fetal bovine serum (FBS, Tissue Culture Biologicals) and 1% Antibiotic-Antimycotic (GIBCO) in a 5% CO_2 humidified atmosphere.

Rat Hippocampal Neuron Culture

Cultured primary hippocampal neurons were prepared from the brains of embryonic day 18 (E18) Sprague-Dawley rats (Koateck), as previously described (Um et al., 2014). Neurons were seeded onto 25-mm poly-L-lysine (1 mg/ml) coated coverslips and cultured in neurobasal media (GIBCO) supplemented with 2% B-27 (GIBCO), 0.5% FBS (Hyclone), penicillin-streptomycin and 0.5 mM Gluta-Max (GIBCO). All procedures were performed according to the guidelines and protocols for rodent experimentation provided by the Institutional Animal Care and Use Committee (IACUC) of KAIST and DGIST.

METHOD DETAILS

Proteins Expression and Purification

The extracellular domain of human NL2 (aa 42P–610N) was cloned into modified pAcGP67 vector (GE Healthcare Life Sciences) containing the protein A gene derived from pEZZ18 (GE Healthcare life Sciences), whereas the extracellular domain of MDGA1 Ig1-3 (aa 19Q–330K) was cloned into modified pAcGP67 vector containing the Fc domain of human IgG. The N-glycosylation site (N98) of NL2 was mutated to glutamine (N98Q) to facilitate crystallization. A thrombin cleavage sequence (LVPRGS) was introduced between the target gene (NL2 or MDGA1 Ig1-3) and the genes encoding the affinity tag. High Five insect cells (Invitrogen) were infected with P4 baculovirus containing these constructs and incubated at 28°C for 3 days. After pelleting the cells by centrifugation, the supernatants containing secreted Protein A-fused NL2 were loaded onto IgG Sepharose resin (GE Healthcare Life Sciences), whereas the supernatants containing secreted Fc-fused MDGA Ig1-3 were loaded onto Protein A Sepharose resin (GE Healthcare Life Sciences). The protein-bound resins were washed with 10mM HEPES, pH 7.5, 150mM NaCl and incubated with thrombin (1% (v/v) in 10mM HEPES, pH 7.5, 150mM NaCl, at 4°C overnight to remove the C-terminal Protein A and Fc tags. NL2 was dialyzed against 20mM HEPES, pH 7.0, loaded onto a anion-exchange HiTrap Q column (GE Healthcare Life Sciences) and eluted with a 0–1M NaCl gradient. MDGA Ig1-3 was dialyzed against 20mM MES, pH 6.5, loaded onto a cation-exchange HiTrap SP column (GE Healthcare Life Sciences) and eluted with a 0–1M NaCl gradient. Fractions containing recombinant proteins were further purified by gel-filtration chromatography on Superdex 200 columns (GE Healthcare Life Sciences) equilibrated with 10mM HEPES, pH 7.5, 150mM NaCl. The NL2/MDGA1 Ig1-3 complex was produced by incubating purified NL2 (dimer) and MDGA1 at 1:2 stoichiometry overnight at 4°C, followed by gel filtration chromatography on a Superdex 200 column (GE Healthcare Life Sciences) equilibrated with 10mM HEPES, pH 7.5, 150mM NaCl to remove unbound MDGA1 Ig1-3. Fractions containing the NL2/MDGA1 Ig1-3 complex were concentrated to 10mg/ml for crystallization.

To obtain recombinant Nrx1β-Fc for cell surface binding assays (Figure 2D), the extracellular domain of human Nrx1β (51A–269S) was cloned into a modified pcDNA3.1 vector containing the N-terminal signal sequence and the C-terminal Fc domain of human IgG. To label Nrx1β-Fc with Cy5, S396 in the Fc domain was mutated to Cys by QuikChange site-directed mutagenesis (Stratagene). Using polyethylenimine (PEI), this construct was transfected into HEK293F cells grown in suspension (Vink et al., 2014). The cells were harvested after 3 days and pelleted by centrifugation, and the supernatants containing Nrx1β-Fc (S396C) were loaded onto Protein A Sepharose (GE Healthcare Life Sciences). Nrx1β-Fc (S396C) was eluted with 100 mM glycine, pH 3.5, and the solution was immediately neutralized with 100 mM Tris-HCl (pH 8.0) and subjected to gel filtration chromatography on a Superdex 200 column (GE Healthcare Life Sciences) in 10mM HEPES, pH 7.5, 150mM NaCl.

To obtain recombinant proteins for use in biolayer light interferometry (BLI) experiments (Figure 4A), human NL1AB (46Q-634N), NL1A (46Q-634N, -ssB: 295G-303K), NL2 (15Q-610N), full-ecto MDGA1 (19Q-919K), MDGA1 Ig1-3 (19Q-330K), full-ecto MDGA2 (20Q-914K), and Nrx1β (51A–269S) were cloned into a modified pcDNA3.1 vector containing the N-terminal signal sequence and the C-terminal Fc domain of human IgG. A thrombin cleavage sequence (LVPRGS) was introduced between the target gene and the genes encoding the affinity tag (Fc domain). The constructs were transfected into HEK293F cells, which were cultured for 3 days, and pelleted by centrifugation. The culture supernatants were loaded onto Protein A Sepharose resin, and the C-terminal Fc domain was removed by on-column thrombin digestion (1% (v/v) in 10mM HEPES, pH 7.5, 150mM NaCl) at 4°C overnight. The eluted proteins were further purified by gel filtration chromatography on Superdex 200 columns in 10mM HEPES, pH 7.5, 150mM NaCl.

To obtain recombinant rNL1-Fc and rNL2-Fc proteins for use in pull-down analyses (Figures 4B and 4C), HEK293T cells grown to 80% confluence in 10-cm dishes were transfected using calcium phosphate with 20 μg of the rNL1-Fc and rNL2-Fc constructs (Lee et al., 2013). Media were harvested 4 days later and cleared by centrifugation at 1,000 x *g*. The supernatants were dialyzed against 10 mM HEPES-NaOH, pH 7.4, 1 mM EDTA, and protease inhibitors (Roche Applied Science), and incubated overnight with protein A-Sepharose to purify rNL1-Fc AND rNL2-Fc. The resin was washed to remove unbound proteins, and the bound proteins were eluted with 0.1 M glycine, pH 3.5. The purified proteins were quantified by Coomassie-blue stained gel analyses using bovine serum albumin as a standard.

Glycosylation Site Analysis

Peptides resulting from non-specific digestion were prepared as previously described (Hua et al., 2013). Briefly, 50 μg/μL neuroligin-2 was incubated with 50 μg/μL pronase E for 1 hr at 37°C. The digested peptides were enriched by graphitized carbon solid-phase extraction (GC-SPE) and analyzed by nanoLC-Chip Q-TOF MS (Agilent Technologies). The LC-MS and MS/MS data were processed and identified as previously described using MassHunter Qualitative Analysis software (version B.06.00, Agilent Technologies) and GP Finder software (An et al., 2006).

Crystallization and Structural Determination

Crystals of NL2/MDGA1 Ig1-3 complex were grown for 1 week using the hanging-drop vapor-diffusion method, in which 1μl of protein complex (10mg/ml) was mixed with 2μl of crystallization buffer containing 300mM ammonium citrate tribasic, pH 7.0, 13% 1,3-butanediol and 18% PEG3350 (v/v). Crystals of the NL2/MDGA1 Ig1-3 complex belonged to space group C2 and had the following unit cell constants: a = 154.88Å, b = 69.14Å, c = 108.84Å, α = 90.00°, β = 115.31° and γ = 90.00°. For data collection at

100K, the crystals were transferred to a cryoprotective solution containing 300mM ammonium citrate tribasic, pH 7.0, 13%1,3-butanediol and 25% PEG3350 (v/v), and shock frozen in liquid nitrogen. After collecting diffraction data at beamline 5C (Pohang Accelerator Laboratory), the data were reduced and integrated using XDS (Kabsch, 2010). Three collected datasets were merged using Blend (Foadi et al., 2013) and the initial phases were calculated by the molecular replacement technique using PHASER (McCoy et al., 2005). The structures of mouse neuroligin-2 (PDB: 3BL8) and the Ig-like domain of human BTLA-HVEM complex (PDB: 2AW2) were used as search probes for structure determination. Iterative rounds of manual model building were performed using Coot (Emsley and Cowtan, 2004), with refinement by PHENIX (Adams et al., 2002) (Table S1). A Ramachandran plot analysis of the NL2/MDGA1 Ig1-3 complex structure that showed 95.0%, 4.7%, and 0.2% of residues were in favored, allowed, and outlier regions, respectively. All structural figures were depicted using PyMOL (Molecular Graphics System).

Cell Adhesion Assays

Two groups of L cells (ATCC) in 6-well plates were transfected with 1-2 μg of the indicated expression vectors (Figure 2B). After 30 hr, the cells were trypsinized and resuspended in DMEM, supplemented with 10% FBS and 1% penicillin/streptomycin. L cells expressing EGFP and WT or variant NL2 were mixed with L cells expressing DsRed and WT or variant MDGA1 Ig1-3. The cell suspensions were rotated at room temperature for 1 hr to allow the cells to aggregate. The cells were subsequently spotted onto 8-well culture slides (SPL), and the extent of cell aggregation was assessed with confocal microscopy (LSM510, Zeiss).

Cy5-Nrx1β-Fc Binding Assays on Cell Surfaces

HEK293T cells were seeded onto coverslips in 12-well plates and transfected with 0.5 μg of pEGFP-NL2-PDGFR TM, alone (control) or together with 0.5 μg of an indicated pDis-HA-MDGA1 full variant. After 48 hr, the cells were fixed with 4% paraformaldehyde for 15 min at room temperature and incubated overnight at 4°C with mouse anti-HA antibody (Sigma Aldrich, 1:500) under non-permeabilized conditions, followed by incubation with Cy3-conjugated donkey anti-mouse IgG (H+L) (Jackson ImmunoResearch, 1:500) to visualize surface HA-MDGA1 variants. To assess the effects of MDGA1 variants on NL2/Nrx-1β binding, cells expressing NL2 and each HA-MDGA1 full variant were treated with 20 μg/ml Cy5-labeled Nrx1β-Fc in phosphate buffered saline (PBS) containing 2 mM $CaCl_2$ for 3 hr at room temperature and washed three times with PBS containing 2 mM $CaCl_2$. Nrx1β-Fc was labeled with Cy5 maleimide mono-reactive dye (GE Healthcare) according to the manufacturer's protocol and separated from any remaining free dye by Bio-Gel p6 DG gel filtration chromatography (Bio-Rad). Images were acquired using a confocal microscope (LSM780, Carl Zeiss) (Figure 2D).

Heterologous Synapse-Formation Assays

Heterologous synapse-formation assays using HEK293T cells (ATCC) were performed as previously described (Um et al., 2014). For the experiments shown in Figure 2D, HEK293T cells were co-transfected with pEGFP-NL2-PDGFR TM (NL2-EGFP) and WT or mutant pDis-HA-MDGA1 using Lipofectamine 2000 (Invitrogen). After 24 hr, the cells were trypsinized, seeded onto hippocampal neuron cultures at DIV10 and co-cultured for an additional 24 hr. At DIV11, the cells were incubated with antibodies against EGFP (Rockland; 1 μg/ml), Synapsin (JK014; 1:1000) (Han et al., 2016), and HA (Covance; 1 μg/ml), followed by incubation with Cy3-, FITC-, and Cy5-conjugated secondary antibodies (Jackson ImmunoResearch). Images were acquired by confocal microscopy (LSM700, Carl Zeiss) (Figure 2F).

Size Exclusion Chromatography

To analyze the competitive binding of MDGA1 and Nrx1β to NL2, the NL2/MDGA1 Ig1-3 complex was incubated with Nrx1β (Figure 3B), and the NL2/Nrx1β complex was incubated with MDGA1 Ig1-3 (Figure 3C) at molar ratios of 1:1 and 1:5 in the presence of 2 mM $CaCl_2$ at 4°C for 3 hr. These mixtures were applied to a Superdex 200 10/300 GL column (GE Healthcare Life Sciences) in buffer containing 10 mM HEPES, pH 7.5, 150 mM NaCl, and 2 mM $CaCl_2$. Gel filtration fractions were analyzed by SDS-PAGE and visualized by Coomassie blue staining (Invitrogen). To access the Ca^{2+}-dependence of the competitive binding of MDGA1 and Nrx1β to NL2, the NL2/MDGA1 Ig1-3 complex was incubated with Nrx1β, and the NL2/Nrx1β complex was incubated with MDGA1 Ig1-3 at 1:1 molar ratios in the presence of 10 mM EDTA, followed by size exclusion chromatography in buffer containing 10 mM HEPES, pH 7.5, 150 mM NaCl, and 10 mM EDTA.

Determination of Binding Kinetics

The binding kinetics of MDGAs and Nrx1β to NLs were measured by biolayer light interferometry (BLI) on an Octet RED96 system (ForteBio, Pall Life Sciences) (Figure 4A). The mixtures were agitated at 1,000 rpm in washing buffer (10 mM HEPES, pH 7.5, 150 mM NaCl, 2mM $CaCl_2$). Assays were performed at 30°C in solid black 96-well plates (Geiger Bio-One), with each well containing a final volume of 200 μl. Biotinylated NL1AB, NL1A, and NL2, at concentrations of 1 μg/ml, were loaded onto the surfaces of streptavidin biosensors (ForteBio) for 1 min, followed by washing of the loaded biosensors for 2 min with washing buffer (10 mM HEPES, pH 7.5, 150 mM NaCl, 2 mM $CaCl_2$) to remove any unbound protein. The biosensor tips were immersed in wells containing serial dilutions of MDGA1, MDGA2, or Nrx1β, starting at maximum concentrations of 500 nM for MDGAs and 2 μM for Nrx1β. NL-MDGA associations (on rate, kon) were measured over a 5 min interval. The sensors were subsequently immersed in washing buffer for 5 min to measure dissociation (off-rate, koff). K_D, measured in nanomoles, was calculated as the ratio of off-rate to on-rate

(koff/kon). As dimeric NL2 contains two binding sites for MDGA1, with the binding to MDGA1 at each site being independent and having a different rate constant, the resulting data were analyzed by fitting to a 2:1 heterogeneous ligand model with the global fitting function (grouped by color, Rmax). A similar method was used to measure binding affinity of Nrx1β to NL2. The sensograms were corrected using the blank reference and fit with the ForteBio Data Analysis software 9.0.

Generation of Polyclonal Antibody to MDGA1

MDGA1 peptide (SRPRELGDRARLVSPLYC; constituting amino acids 802 - 818 of mouse MDGA1), was synthesized and conjugated via its C-terminal cysteine residue to keyhole limpet hemocyanin. Rabbits were injected with the conjugated peptide to generate MDGA1-specific polyclonal antibody (JK030, Abfrontier [Cat. No.: AR15-PA0001]; see Figures S4A and S4B for characterization of this in-house produced MDGA1-specific antibody). The resulting antisera were affinity purified on SulfoLink columns (Pierce), with the resulting antibodies used in immunoblotting experiments.

Pull-Down Assays

HEK293T cells were transfected with pGW1-HA-MDGA1, pGW1-HA-MDGA2, or pCAG-FLAG-Nrx1β, harvested 48 hr later and incubated for 1 hr at 4°C in solubilization buffer (25 mM Tris-HCl, pH 7.6, 150 mM NaCl, 1% NP-40, 1% sodium deoxycholate, 0.1% sodium dodecyl sulfate, 5 mM $CaCl_2$, 5 mM $MgCl_2$). The suspension was centrifuged at 20,000 x g to remove insoluble debris, and each supernatant was mixed with 10 μg rNL1-Fc, rNL2-Fc, or Fc (control) supplemented with protein A-Sepharose beads and incubated at 4°C for 2 hr with gentle agitation (Figure 4C). For in vivo pull-down assays, synaptosomal fractions prepared from mouse brains (P14) were mixed with 10 μg MDGA1-Fc or Fc (control) and incubated at 4°C for 4 hr with gentle agitation (Figure 4D). Protein A beads were washed three times with solubilization buffer, solubilized in SDS sample buffer, and loaded onto 8% SDS-polyacrylamide gels for immunoblot analyses. The antibodies used for immunoblotting were anti-HA, anti-FLAG, anti-NL1, anti-NL2, anti-MDGA1, anti-TrkC, and anti-PSD-95, each at a concentration of 1 μg/ml.

QUANTIFICATION AND STATISTICAL ANALYSIS

Cell Adhesion Assay

Cell aggregates were defined as two or more cells, with at least one green (EGFP) and one red (DsRed) cell. The area of each aggregate was measured using the MetaMorph software (Molecular Devices) and reported as the mean ± SEM of 12 - 15 fields from at least three independent experiments, with statistical significance assessed with the non-parametric Kruskal-Wallis test. Areas smaller than the average size of a single cell were excluded from analysis.

Nrx1β Binding Assays on Cell Surfaces

For quantification, the ImageJ (NIH) software was used. The intensity of the Cy5 signal of bound Nrx1β-Fc was normalized to the fluorescence intensity of NL2-EGFP. Only cells co-expressing NL2-EGFP and the indicated MDGA variants were chosen for quantification. Data are shown as the mean ± SEM of 15 HEK293T cells from at least three independent experiments, with statistical significance assessed with the Kruskal-Wallis test.

Heterologous Synapse-Formation Assays

In quantifying the acquired images, the contours of the transfected HEK293T cells were defined as the region of interest. The fluorescence intensity of the immunoreactive synapsin puncta were normalized relative to each HEK293T cell area, with the normalized signal ratio quantified by the MetaMorph software (Molecular Devices). Data are presented as mean ± SEM of 15 - 22 HEK293T cells per experimental condition, with statistical significance assessed with the Kruskal-Wallis test, followed by Dunn's post hoc tests, using cell numbers as the basis for 'n'.

DATA AND SOFTWARE AVAILABILITY

Data Resources

The accession number for the coordinate of human NL2/MDGA1 Ig1-3 complex reported in this paper is PDB: 5XEQ.